

M. Schubert · J. Perlwitz · R. Blender · K. Fraedrich
F. Lunkeit

North Atlantic cyclones in CO₂-induced warm climate simulations: frequency, intensity, and tracks

Received: 27 January 1998 / Accepted: 19 May 1998

Abstract The effect of CO₂-induced climate change on the North Atlantic storm and cyclone tracks in winter is analysed using time slice experiments of the Hamburg atmospheric general circulation model (ECHAM3) with triangular truncation at wave number 42 (T42) and 19 levels. The sea surface temperature (SST) and sea ice boundary conditions for these experiments are taken from a transient Intergovernmental Panel on Climate Change (IPCC) scenario A run of ECHAM1/LSG at the times where the 1 × CO₂ (control run), the 2 × CO₂ and the 3 × CO₂ concentrations are reached. Using a cyclone identification and tracking scheme, we detect the low pressure systems as relative minima in the 1000 hPa geopotential height field and connect them to cyclone tracks. The results of the Eulerian analysis of the storm track using filtered variances and the Lagrangian analysis of the cyclone trajectories from the three climate runs are discussed and compared with each other. In the 2 × CO₂ experiment, the storm track shifts eastward, whereas the cyclone density shifts northeastward. In the 3 × CO₂ experiment the storm track shows a southeastward shift, whereas the cyclone density shifts northward. The variability of the cyclone tracks is determined by a cluster analysis of their relative trajectories considering the first three days of the cyclones. The relative cyclone tracks are grouped into stationary, zonal and northeastward travelling cyclones. This analysis provides a method to assess the model quality and to detect changes of the cyclone trajectories in different climates. In the 2 × CO₂ (but not in the 3 × CO₂) run the occupation number of northeastward cyclones increases.

1 Introduction

Global warming caused by anthropogenic emissions of greenhouse gases may have an impact on a variety of climatic variables such as temperature, wind, and precipitation with changes not only in the mean quantities but also in the variability. In the midlatitudes cyclones are the most dominant phenomena; they contribute the largest part of precipitation and are associated with extreme storms and floods. The European climate is predominantly determined by the cyclones originating over the North Atlantic, and is supposed to react sensitively to SST changes in this region.

A response of the observed global mean temperature to the influence of the greenhouse effect is widely accepted and supported by objective analysis (Hegerl et al. 1996). Flohn et al. (1992) detect a trend of the tropospheric water vapour content, accompanied by an accelerated hydrological cycle, and an intensification of the tropospheric circulation in the Northern Hemisphere. A change of the observed midlatitude cyclones, however, is still in question. Schinke (1993) detects a positive trend of the number of deep cyclones over Europe and the North Atlantic in the period 1930–1991. Lambert (1996) observes an increase of intense cyclones predominantly after 1970 in the whole Northern Hemisphere. Zishka and Smith (1980), however, find a decrease of the total number of cyclones and a deepening of the central pressure, whereas von Storch et al. (1993) cannot prove evidence for an increasing storminess during the last 100 ys. A final confirmation of the modification of the observed climate does not seem to be possible mainly due to sparse and inconsistent data, and due to the lack of long time series. GCM simulations provide a tool to estimate possible anthropogenic climate changes utilising a comprehensive data set. In recent years several investigations have addressed this problem using output from global coupled models or from time slice experiments with

M. Schubert · J. Perlwitz¹ · R. Blender · K. Fraedrich (✉) · F. Lunkeit
Meteorologisches Institut, Universität Hamburg,
Bundesstr. 55, D-20146 Hamburg, Germany
E-mail: blender@dkrz.de

Present address:

¹Department of Applied Physics, Columbia University,
NASA/GISS, 2820 Broadway, New York, NY 10025, USA

atmospheric models. The majority of the analyses show a qualitatively consistent CO₂-doubling or tripling response of the mean temperature distribution. However, the predicted modifications of higher moments such as the cyclonic activity are less clear, mainly because the detected changes are small and seem to depend on the detailed structure of the time mean fields (IPCC 1992).

The cyclonic activity is analysed by different approaches. The most common way is to determine the storm track, defined by an area of enhanced variance of band-pass filtered 500 hPa geopotential height fields (Blackmon 1976). Another method considers the intensity and spatial distribution of individual low pressure systems without connecting them to trajectories. Based on these data, the Lagrangian technique determines the tracks of individual cyclones during their life cycles. Time mean distributions based on cyclone tracking must be different from the storm track analysis because (a) anticyclones are not incorporated, and (b) because a condition for a minimum life time is typically required. Therefore, the storm track is no more than an indicator for the cyclone frequency. The results of different cyclone tracking algorithms may vary significantly because they depend on the method used (next neighbour search or variational, see e.g. Hodges 1994), on the type of grid data available, on the spatial and temporal resolution, on criteria for the intensity of the lows detected, on assumptions concerning the transporting wind and maximum velocities of the cyclones, and on conditions pertaining to the minimum life time and intensity. Most investigations on changes of the cyclonic activity in GCM simulations concentrate on the northern hemispheric winter season. The models are difficult to compare because they differ with respect to the representation of the ocean (slab ocean, time slice, or interactively coupled), the horizontal resolution, parametrisation schemes, and the prescribed amount of the greenhouse gas concentration. Together with individual systematic errors of the models this leads to significant differences between the simulated time mean state. The following related studies are briefly summarised.

Siegmund (1990) analyses the storm track in a coupled atmosphere-slab ocean model and finds a northward shift over the North Atlantic and over the Northern Pacific ocean in the $2 \times \text{CO}_2$ experiment. In contrast, Stephenson and Held (1993) find a marked weakening of the North Atlantic storm track in a $2.5 \times \text{CO}_2$ atmosphere in a time slice simulation based on a transient coupled ocean atmosphere simulation. König et al. (1993) analyse the impact of global warming on the cyclone tracks in a T21 (triangular truncation at zonal wave number 21) scenario (IPCC scenario A) simulation. They do not find significant changes in the cyclone frequency. König et al. (1993) get a poleward shift of the North Atlantic storm track. The cyclone tracking method is based on the 1000 hPa

geopotential height and the 850 hPa vorticity fields in 12 h and 24 h temporal resolution. A minimum life time of one day and a minimum intensity are required. This method is used with slight modifications by various other authors. Hall et al. (1994) find a northward shift and an eastward extension of the North Atlantic storm track in a coupled atmosphere slab ocean model ($2.5^\circ \times 3.75^\circ$ resolution) for $2 \times \text{CO}_2$. Lambert (1995) detects little changes in the frequency of lows. Carnell et al. (1996) investigate the cyclonic activity in coupled model simulations ($2.5^\circ \times 3.75^\circ$ resolution) for the present day and double CO₂ climate and compare the storm tracks (based on the variance) with the cyclone frequencies obtained by the method of König et al. (1993). The results differ in the response of the North Atlantic storm track; the $2 \times \text{CO}_2$ experiment shows a downstream extension and a northward shift, whereas the cyclone frequency shows no downstream extension. Lunkeit et al. (1996) combine several diagnostic tools to assess changes of cyclonic activity simulated in a transient coupled greenhouse simulation: zonal mean structure, storm tracks, Eady growth rate, and cyclone frequency using the method of König et al. (1993). In the North Atlantic region consistent results show an enhanced cyclonic activity at the eastern tail of the storm track and a northward shift of the storm track axis.

Beersma et al. (1997) analyse a high resolution (T106) ECHAM3 scenario and compare the control run with ECMWF analyses. The high resolution makes the determination of extreme events possible, but the short duration of the simulations (5 y) is well below the climatic time scale and prohibits evidence for climate change. The authors find slight differences between the control run and the $2 \times \text{CO}_2$ simulation, with a shift of deep depressions to the North Sea and the Bay of Biscay. Zhang and Wang (1997) analyse a NCAR-CCM/slab ocean scenario experiment to compare control and $2 \times \text{CO}_2$ conditions. They find a negative anomaly of the storm track in the Northern Atlantic, no significant change of the frequency of lows, and a decrease of the frequency of anticyclones in this region.

In summary, there is some evidence for a northward shift and an intensification, but possibly also an eastward extension of the North Atlantic storm track due to increased greenhouse gas concentrations. The Northern Pacific storm track seems to be less sensitive. The various investigations yield remarkable differences possibly caused by differences of the experimental design and the diagnostic methods. Even storm track and cyclone track analyses can show deviations in the changes of the cyclonic activity when they are applied to the same data set (Carnell et al. 1996).

Here we investigate the impact of increased greenhouse gas concentrations on the North Atlantic storm track and the cyclone tracks in time slice experiments with the T42 version of the Hamburg atmospheric

general circulation model ECHAM3 (Perlwitz 1997). The SST boundary conditions are monthly means based on two runs of the coupled T21 atmosphere ocean model ECHAM1/LSG (Cubasch et al. 1992), a present-day control run, and a transient greenhouse warming simulation (IPCC scenario A). Time slice experiments are performed for $1 \times \text{CO}_2$, $2 \times \text{CO}_2$, and $3 \times \text{CO}_2$ conditions. We use traditional storm track measures and individual cyclone track analysis. The cyclone tracks are extracted and analysed by a cluster analysis of the relative trajectories which has been applied to identify cyclone track regimes in observations (Blender et al. 1997). The cluster analysis groups the cyclone trajectories in stationary, zonal and north-eastward travelling cyclones with different physical properties. The motivation for the present study is to detect changes in the cyclonic activity by considering the variability of the individual cyclone tracks using this approach.

The work is outlined as follows: in Sect. 2 we describe the scenario A and the three time slice experiments. In Sect. 3 the result for the zonal mean temperature and the storm track statistics in the three runs are presented. Sect. 4 comprises the method and the results of the Lagrangian cyclone track analyses. In the final Sect. 5 the results are summarised and discussed.

2 The scenario experiments

Data of a time slice experiment are analysed, produced by the T42/L19 ($2.8^\circ \times 2.8^\circ$) resolving version of the atmosphere model ECHAM3 (Roeckner et al. 1992; Cubasch et al. 1995; Perlwitz 1997). In these experiments, the model is forced by annual cycles of global SST anomalies obtained from climate change integrations (Cubasch et al. 1992) of the T21 resolving coupled ocean-atmosphere model ECHAM1/LSG. The atmospheric part of the coupled model is the ECHAM1 (Roeckner et al. 1989) and the ocean part is the Large-Scale Geostrophic model (LSG, Maier-Reimer and Hasselmann 1987). The SSTs for the time slice experiments are extracted from two coupled model experiments, a control run and a transient greenhouse warming scenario (Cubasch et al. 1992). The integration time of both runs is 100 y; in the control experiment, the CO₂ concentration has the constant value of 330 ppm. In the scenario, the increased CO₂ concentration is defined according to the IPCC Scenario A (IPCC 1990).

For the time slice experiments, two 10 y intervals are chosen from the Scenario A experiment to extract the SSTs. The first one is centred around the year with a CO₂ concentration of twice the value of the control. The second interval is the last decade of the Scenario A experiment, where the CO₂ concentration attains about three times the value of the control experiment. For each month of the year, the 10 y mean of the SST is determined for both the $2 \times \text{CO}_2$ and $3 \times \text{CO}_2$ scenario. Thus, interannual fluctuations are eliminated to obtain a mean annual cycle representing the mean state of the SST according to the CO₂ concentration at this time. Next, an annual cycle of SST anomalies is calculated for $2 \times \text{CO}_2$ and $3 \times \text{CO}_2$ using the difference between the SST, extracted from the Scenario A experiment, and the 10 y mean of the SST, derived from the first decade of the control experiment. After interpolation to higher resolution, the anomalies are added to a climatological SST, estimated from observations between 1979 and 1988 (Atmospheric Model Intercomparison Project or AMIP, Gates 1992). The result-

ing new SSTs are used as lower boundary conditions for the time slice experiments, carried out for $2 \times \text{CO}_2$ and $3 \times \text{CO}_2$, with the uncoupled atmospheric model. Annual cycles of the mean sea ice distribution are also prescribed as a lower boundary condition in the time slice experiments both for $2 \times \text{CO}_2$ and $3 \times \text{CO}_2$. They are equal to the 10 y mean of the sea ice distributions in the transient Scenario A experiment (Cubasch et al. 1992), in the decades from which the SSTs are extracted. The 30 y integration of the time slice experiments follows after an integration of three model years, which is carried out to avoid a bias by an initial trend. The prescribed CO₂ concentration is 690 ppm for the $2 \times \text{CO}_2$ experiment and 1045 ppm for the $3 \times \text{CO}_2$ experiment. The time slice experiments are compared with a control experiment, having 100 integrated model years. In this run, the climatological AMIP SST is taken as a lower boundary condition and the prescribed CO₂ concentration is 345 ppm.

Figure 1a shows the SST in Northern Hemispheric winter (DJF) used in the control experiment, and the SST anomalies prescribed in the time slice experiments for $2 \times \text{CO}_2$ Fig. 1b and $3 \times \text{CO}_2$ Fig. 1c. In the time slice experiments, there are local maxima of the forcing which amount to about 1 K for $2 \times \text{CO}_2$ and 2 K for $3 \times \text{CO}_2$, in the tropics and subtropics. In the higher latitudes, the SST increases largely in regions with ice retreat. The coupled model experiment, from which the SST anomalies are extracted, shows that south of Greenland and in the North Pacific, the SST anomalies have minima, which are caused by a reduced exchange of deep and surface water (Cubasch et al. 1994). Both SST forcing patterns are similar. The area weighted correlation coefficient between the prescribed Greenland and North Pacific SST anomalies amounts to 0.85.

3 Eulerian statistics

The time-mean properties of the simulations, that is the first and second moments, which are related to changes in the zonal mean temperature distribution and the eddy activity are briefly discussed (for more details see Perlwitz 1997).

3.1 Temperature

The zonal time-mean cross sections of the temperature in the control experiment and of the responses in the two scenario experiments are presented for Northern Hemispheric winter (DJF, Fig. 2), the shaded areas in the response plots show statistically significant changes based on the 99.9% level of an univariate local t-test. Both scenarios reveal a significant maximum of the warming in the upper tropical troposphere; this maximum is twice as large in the $3 \times \text{CO}_2$ compared to the $2 \times \text{CO}_2$ experiment. In the $2 \times \text{CO}_2$ experiment, the enhanced temperature of the tropical and subtropical mid-troposphere leads to a stronger meridional temperature gradient in the midlatitudes. In the northern high latitudes, a polar warming maximum occurs in the lower troposphere with a maximum at the surface. In the $3 \times \text{CO}_2$ experiment, the polar warming is much larger than in the $2 \times \text{CO}_2$ experiment extending from the surface to the mid-troposphere. That is, in the midlatitudes the meridional temperature gradient of the mid-troposphere remains unchanged in the $3 \times \text{CO}_2$ compared to the $2 \times \text{CO}_2$ experiment.

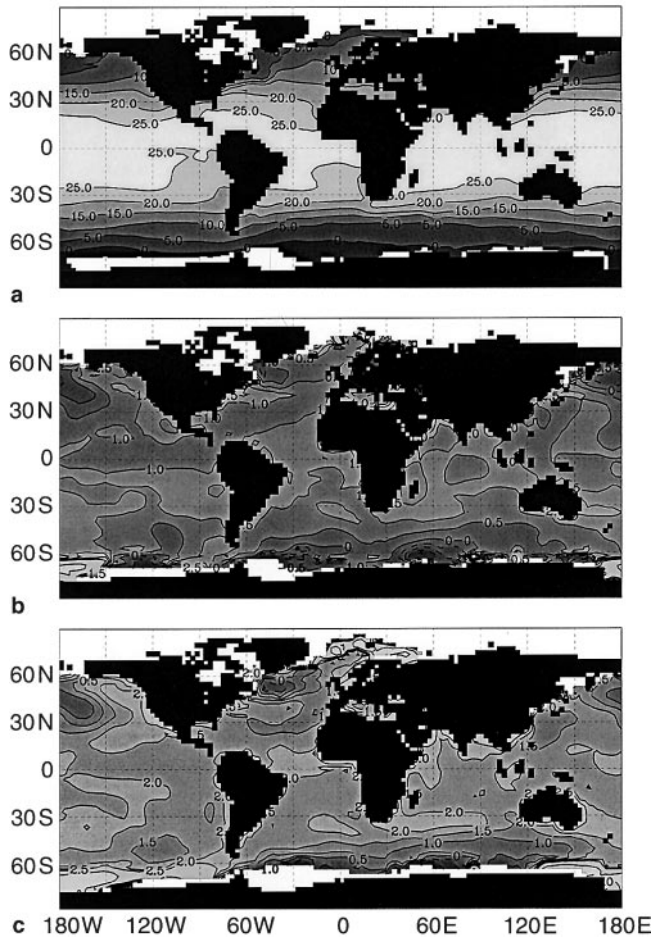


Fig. 1a–c The SST in winter (DJF), **a** used in the control experiment **b** the SST anomalies in the time slice experiments for $2 \times \text{CO}_2$ (**b**) and $3 \times \text{CO}_2$ (**c**). Sea ice is white. Contour intervals are **a** 5° , **b**, **c** 0.5° ; negative contours are dashed

3.2 Storm track

Figure 3a shows the standard deviation of the 500 hPa geopotential height caused by high frequency (2.5–6 days) transient eddies for the control experiment in winter. The results of the $2 \times \text{CO}_2$ and $3 \times \text{CO}_2$ time slice experiments are presented in Fig. 3b,c. The statistical significance of the changes, tested by a simple univariate *t*-test (95% level), is indicated by the shaded areas. There are two maxima of the variability in the control experiment: over the North Atlantic (60 gpm), and over the North Pacific ocean (55 gpm), with values about 20% too low compared to the observations.

The main responses of the enhanced greenhouse gas are located in the North Atlantic and the North Pacific regions. Both time slice experiments show a larger maximum of the variability compared to the control experiment where it is situated east of Newfoundland. The largest increase is located east of the storm track maximum in the eastern North Atlantic, where the

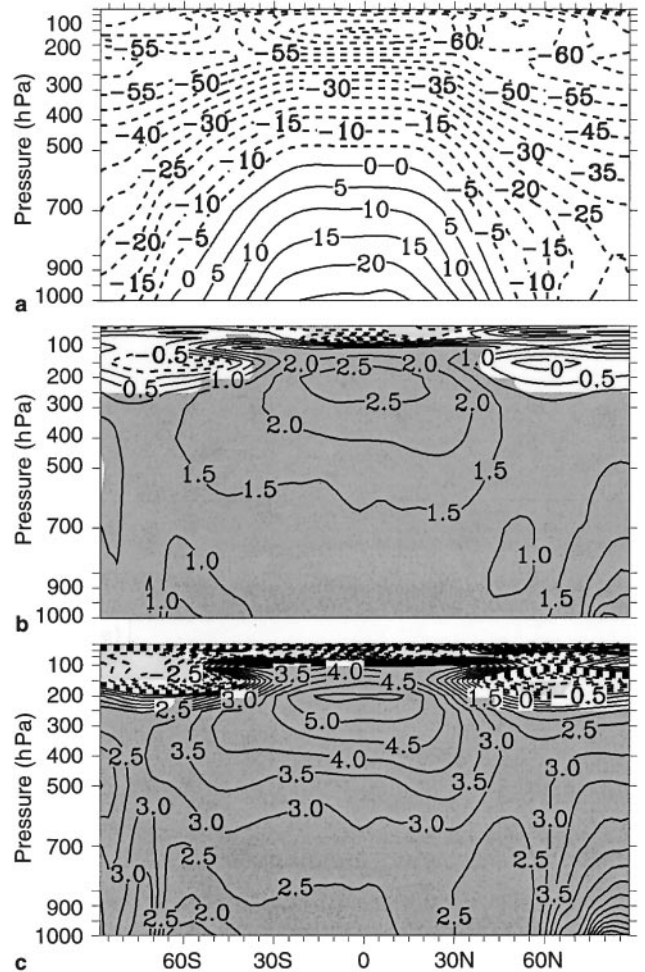


Fig. 2a–c Zonal mean cross sections of the **a** temperature in the control experiment, **b** the deviations in the $2 \times \text{CO}_2$ and the **c** $3 \times \text{CO}_2$ runs. Contour intervals are **a** 5° in, and **b** 0.5° . Shaded areas show statistically significant changes (dark: increase, light decrease)

enhanced variability is statistically significant in both time slice experiments. Maximum variability in the $2 \times \text{CO}_2$ experiment increases by about 6 gpm, which is a 15% rise compared to the control experiment. The $3 \times \text{CO}_2$ experiment shows no additional increase of this maximum, but a south-eastward extension of the affected area.

A qualitatively similar nonlinear response is found over the North Pacific. The variability is increased by about 10%, compared to the control experiment, in the $2 \times \text{CO}_2$ -experiment south-east of the Pacific storm track maximum. However, there is no additional increase in this region in the $3 \times \text{CO}_2$ -experiment, but a northwestward shift of the maximal significant change and a zonal extension.

The nonlinear behaviour of the geopotential height variability response in the Northern Hemisphere is determined by the mid-tropospheric temperature change pattern, affecting the baroclinicity change

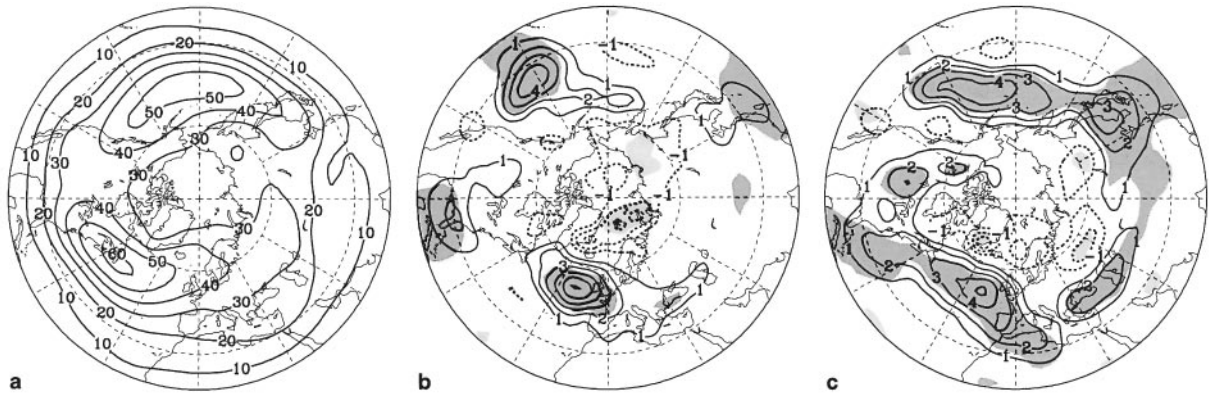


Fig. 3a–c Standard deviation of the 500 hPa geopotential height, **a** control, **b** deviations for $2 \times \text{CO}_2$, and **c** $3 \times \text{CO}_2$. Contour intervals are **a** 10 in and **b**, **c** 1 in. Significant changes are shaded (dark: increase, light: decrease)

(Perlwitz 1997). Regions with a maximum temperature increase, caused by an adiabatic warming in the subsiding branches of the Hadley cell, lie in the subtropical regions in the $2 \times \text{CO}_2$ experiment. Minimal temperature changes are located in the high-latitude troughs over the oceans. The baroclinicity increases for CO_2 doubling in the midlatitudes between the subtropical warming maxima and the high-latitude minima.

The adiabatic warming in the subtropics is much larger in the $3 \times \text{CO}_2$ than in the $2 \times \text{CO}_2$ experiment. However, in contrast to CO_2 doubling, there is a large polar warming for CO_2 tripling in winter caused by the prescribed melting of a substantial amount of sea ice. This polar warming, extending from the surface to the middle troposphere, counteracts the additional baroclinicity enhancement in the $3 \times \text{CO}_2$ experiment in the midlatitudes leading to the nonlinear variability response.

4 Cyclone analysis

Transient eddy statistics combine the effects of high and low pressure systems. The rain-bearing frontal cyclones which determine the water cycle, for example, are analysed by cyclone tracing algorithms. This leads to the determination of the tracks of cyclones from which life cycles, frequency, intensity, and direction can be deduced. This is a first step towards a Lagrangian cyclone climatology.

4.1 Cyclone tracking

The cyclone tracking algorithm proceeds in the following steps (Blender et al. 1997): First, a low is identified as a 1000 hPa geopotential height minimum and by a minimum value of the mean gradient of 5 m/1000 km in a synoptic neighbourhood. The gradient is chosen as the intensity measure instead of the central pressure

because the central pressure changes with the regional climate mean. Secondly, these lows are connected to tracks via a nearest neighbour search within a distance of 1000 km. Finally, it is required that the minimum lifetime lasts 3 days and that a minimum intensity of 20 m/1000 km is reached at least once during the life cycle. Our algorithm differs from the one introduced by König et al. (1993), which has been applied to CO_2 scenarios by other authors, in that the latter one neglects the poleward divergence of the size of the search region in grid-point space. Our method is tested with high resolution (T106) observational data stored in 6 h time intervals, and with a short period of the $2 \times \text{CO}_2$ run stored in 2 h time intervals; both tests show excellent agreement with a subjective analysis. The comparison of the 2 h and 12 h tracks reveals satisfactory 12 h tracks so that the algorithm is used here without further alteration. The following analysis concentrates on the North Atlantic and European region (80°W – 30°E , and 30°N – 90°N) and the winter seasons (DJF). Regions with an altitude higher than 1000 m are excluded. Furthermore, there are no filters applied to exclude stationary cyclones.

4.2 Cyclone frequency

The cyclone frequency is determined by counting the occurrences of the lows which connect to cyclone trajectories. Lows are counted at each time step, even if they remain at the same position. These results cannot be compared to studies which count the lows disregarding their membership to a cyclone life cycle (e.g. Lambert 1995). Since the intense lows are elements of longer-lived cyclones, our result leads to a slight underestimation of a direct low counting. The numbers of cyclones at each T42 grid point are divided by the number of observation times and a unit area. Although area normalisation introduces a bias (Hayden 1981), it is used for possible comparison of cyclone frequencies

in different grids and resolutions. The result is the ratio (in percent) of the temporal occupation of the area 10^6 km² by one or several cyclones. This area is very similar to a 5°-latitude circle with $0.97 \cdot 10^6$ km².

4.2.1 Control run and observations

The cyclone frequency of the control run is shown in Fig. 4a. Distinct frequency maxima, located southeast of Greenland and in the Mediterranean Sea, refer to cyclones predominantly induced by the local topography. Another extended region of enhanced frequency spans from the east coast of North America to northern Europe. It indicates the preferred tracks of the travelling cyclones associated with the North Atlantic storm track. In comparison with the storm track defined by the variance of the 500 hPa geopotential height (Fig. 3a), the cyclone track axis is located northward of the storm track axis; this is also seen in König et al. (1993) and Carnell et al. (1996). While the storm track maximum is localised at the northeast coast of North America, the maximum in the frequency of travelling cyclones is more uniformly distributed inside the storm track region. Differences between the two fields are caused by the anticyclones travelling mainly south-eastward, and by the lack of an intensity measure in the frequency diagram.

The observed cyclone frequency is obtained from ECMWF analyses for the extended winter seasons (Nov–Mar) in 1990–1996 using 6 h time steps (Fig. 4b). Although the observations are available in T106

resolution, the data are analysed in T42, corresponding to the spatial resolution of the T42 time slice experiment. Note, however, that the results are not directly comparable, because the smallest spatial model scale is larger than its resolution. The 6 h resolution of the observations is not reduced to the 12 h resolution of the model data. In the central region of the North Atlantic storm track, the cyclone frequency in the control run (Fig. 4a) is slightly smaller than in the observations (Fig. 4b). Larger differences occur in the area southeast of Greenland and in the Mediterranean, where the frequency of observed cyclones is distinctly higher than in the model simulation. This deviation is due to the ability of the high resolution (T106) analyses to reproduce small-scale properties which are only partially retained in the T42 resolution.

4.2.2 CO₂-scenarios

In the $2 \times \text{CO}_2$ scenario run, the changes of the cyclonic frequency are compared with the $1 \times \text{CO}_2$ control run (Fig. 5a). The significance of the change is indicated with a simple two-sided t-test applied to the variance of the winter to winter variability. The shaded areas mark the 90% significance level. The frequency decreases northeastward of North America at the beginning of the storm track, and increases in a small area in the south-east of Greenland and in a larger area at the end of the storm track. A reduction is found for the Mediterranean cyclones. The region of enhanced cyclone

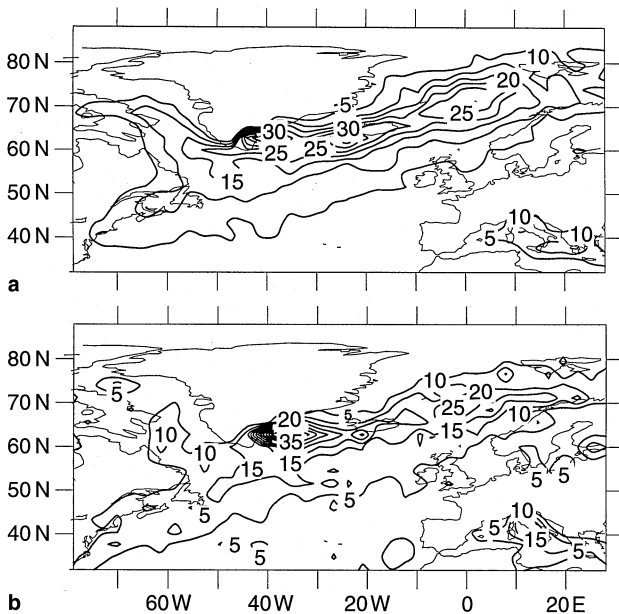


Fig. 4a,b Cyclone frequency (temporal ratio of the occupation in percent) per 1000^2 km² area ($\sim 5^\circ$ -circle) **a** in the control run and **b** the observations; the contour intervals are 5%

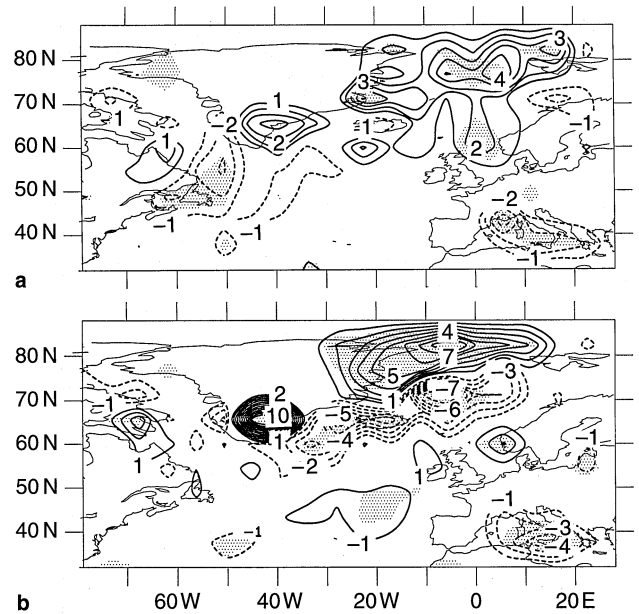


Fig. 5a,b Differences of cyclone frequency (ratio in percent as in Fig. 4) between **a** $2 \times \text{CO}_2$, **b** $3 \times \text{CO}_2$ and the control run; the contour intervals are 1%. Areas of significant deviations are shaded (90% level)

frequency in the vicinity of the storm track is shifted to the northeast.

In the $3 \times \text{CO}_2$ simulation (Fig. 5b), the cyclone frequency at the end of the storm track is significantly reduced compared to the control run. However, there is a considerable increase in a small area near the North Pole. This effect can be explained by the sea ice reduction in the polar sea and the related change in the baroclinicity (see Sect. 3). The reduction of the orographically induced Mediterranean cyclones from $1 \times \text{CO}_2$ to $3 \times \text{CO}_2$ is comparable to the reduction from $1 \times \text{CO}_2$ to $2 \times \text{CO}_2$ (Fig. 5a); only the orographically induced cyclones in the southeast of Greenland, become more frequent in $3 \times \text{CO}_2$.

Comparison of the Fig. 5a and 5b reveals the nonlinearity of the response of the simulated coupled climate system to enhanced greenhouse gas concentrations. Although the drastic reduction of sea ice at $3 \times \text{CO}_2$ might be a specific property of the ECHAM model, the results point out the relevance of the sea ice in the greenhouse warming.

Considerable differences between the anomalies of the storm track (Fig. 3b,c) and the anomalies of the cyclone frequency (Fig. 5a,b) can be noted. In the $2 \times \text{CO}_2$ experiment, the storm track intensifies at the eastward end, whereas the cyclone frequency shifts northeastward. There is no increase of the cyclone frequency in the eastern part of the North Atlantic where the storm track anomaly has its maximum. That is, there is a clear difference between the Lagrangian and the Eulerian transient variability measures. With respect to the cyclone frequency anomalies, the classical storm track (eddy statistics) seems not to be an appropriate indicator. The difference between the storm track and the cyclone frequency is not only due to the anticyclones moving southeastward, also the cyclones (pressure minima) are not directly related to the transient variability. This can clearly be explained by the simple example of superimposing a Rossby wave on a background zonal flow, where the minima disappear when the zonal flow reaches a certain intensity, although the variability remains. However, the spatial structure of the 1000 hPa geopotential height (z_{1000}) anomalies (Fig. 6a,b,c) coincides well with the anomalies of the cyclone frequency. On the other hand, the storm track signal is not reflected in the z_{1000} anomaly.

4.3 Cyclone intensity

An important issue in discussions on the greenhouse effect is a possible cyclone intensity change. Here the strength of the cyclones is measured by the maximum geopotential height gradients during a cyclone life cycle. This gradient is an azimuthal average of the vector gradient around the cyclone centre and determined within the $1000 \text{ km} \times 1000 \text{ km}$ area. The frequencies are determined by the number of cyclones

Table 1 Numbers of cyclones (per month) with maximum gradient within the intervals indicated for the three runs (gradient in $\text{m}/1000 \text{ km}$)

Gradient	Control	$2 \times \text{CO}_2$	$3 \times \text{CO}_2$
< 100	1.42	1.16	1.33
100–200	4.64	4.85	4.88
200–300	4.47	4.57	4.49
> 300	1.62	1.49	1.37
Total	12.15	12.07	12.07

per month and are categorised using the gradient (in units of $\text{m}/1000 \text{ km}$) for each run (Table 1). The weak cyclones (gradient < 100 $\text{m}/1000 \text{ km}$) decrease from $1 \times \text{CO}_2$ to $2 \times \text{CO}_2$, but not from $2 \times \text{CO}_2$ to $3 \times \text{CO}_2$ simulations; cyclones of medium strength (all cyclones between 100 and 300 $\text{m}/1000 \text{ km}$) become more numerous from $1 \times \text{CO}_2$ to $2 \times \text{CO}_2$, but decrease from $2 \times \text{CO}_2$ to $3 \times \text{CO}_2$, and the number of intense cyclones (> 300 $\text{m}/1000 \text{ km}$) decreases. In total, there is only a weak change of the intensities in the scenario runs compared to the control run. The total number of cyclones (disregarding the intensity) cannot be distinguished in the three runs. This result is in some agreement with other results which show that the observed storminess in the North Atlantic region has not altered during the last 100 y (von Storch et al. 1993).

4.4 Cyclone track clusters

The relative cyclone tracks are subjected to a cluster analysis to explore the Lagrangian climatology of cyclone track regimes in the North Atlantic region extending the work of Fraedrich et al. (1990, 1993) and Blender et al. (1997), which describes details of the method applied. The cluster analysis utilises the initial three days of the cyclone trajectories, neglecting short-lived cyclones. The relative distances (dx , dy) of the cyclone positions are scaled by their variances and subjected to the k-means clustering algorithm. For a prescribed number of clusters, the cluster centroids and the grouping is determined by minimising the total distances between the cluster members and their associated centres. The cyclone tracks are grouping into three clusters, which represent northeastward, zonally travelling and stationary cyclones. The clusters of the travelling cyclones are related to particular weather regimes. The life cycles and the mean square displacements within the three clusters show distinct characteristics. The aim of this section is to investigate whether this Lagrangian approach provides a tool to evaluate model experiments and to identify changes of the cyclone activity in scenario experiments.

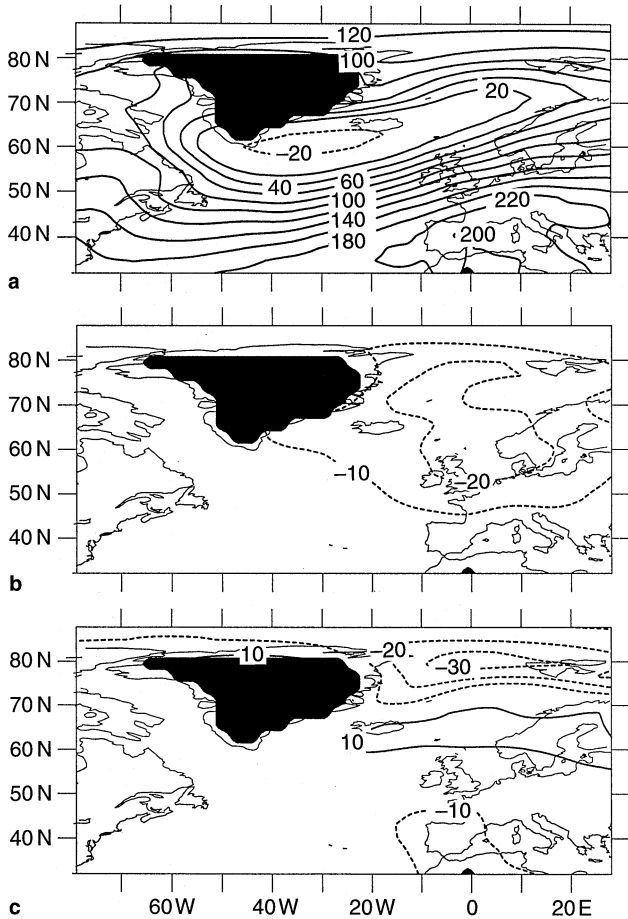


Fig. 6a–c Time mean 1000 hPa geopotential height (in m) **a** in the control run and the anomalies in **b** $2\times\text{CO}_2$ and **c** $3\times\text{CO}_2$. The contour intervals are **a** 20 m and **b,c** 10 m

4.4.1 Control run and observations

Observed cyclone tracks reveal meteorologically meaningful results for three clusters and therefore, three clusters are also used to analyse the model data. First, the control run and the observations are compared. Figure 7 shows the centroids obtained for the cyclones in the control experiment (solid) and the observations (dashed). The horizontal and vertical bars denote the standard deviations of the x and y displacements within the clusters at day 3. Similar to the observations the relative trajectory clusters of the control run separate into northeastward, zonal and stationary regimes. The zonal cluster centroids are different, the northeastward centroids are in remarkable agreement, and the stationary centroids differ little with respect to their zonal extent. The occupation numbers (per month) of the three clusters in the observations (control run) are 4.26 (4.72) in the northeastward, 3.36 (2.88) in the zonal, and 4.4 (4.54) in the stationary cluster. These differences between observations and simulations are due to the

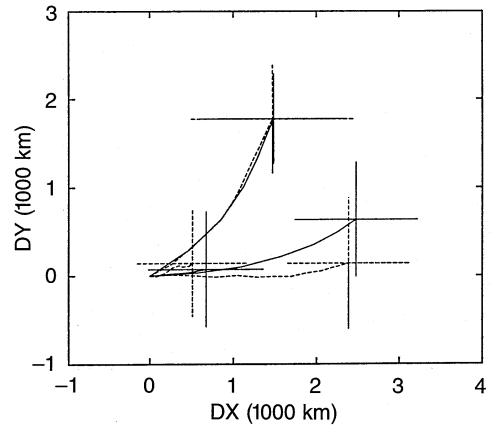


Fig. 7 Cluster centroids of the relative trajectories for the control run (solid) and the observations (dashed). The crosses show the standard deviations within the centroids at 3 days

different shapes of the centroids and are related to shortcomings of the model.

4.4.2 Scenario

The greenhouse effect on the cyclone trajectories is also evaluated by the cluster analysis. First, the analysis is applied to the three runs $1\times$, $2\times$, and $3\times\text{CO}_2$ separately which leads to different sets of centroids (Fig. 8). They show basically the same orientations as in the control run. However, the orientations of the northeastward and the zonal centroids are shifted slightly northward with minor differences between the $2\times\text{CO}_2$ and $3\times\text{CO}_2$ runs. Clearly, the orientation of all travelling cyclones attains a more northward component in the greenhouse gas simulation. An objective comparison of the three runs cannot be made by this type of cluster analysis because both

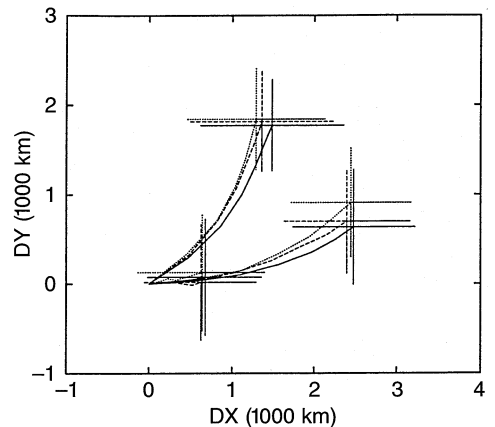


Fig. 8 Cluster centroids for the control (solid), $2\times\text{CO}_2$ (dashed), and the $3\times\text{CO}_2$ (dotted) runs

Table 2 Cluster occupation numbers (per month) in the CO₂ scenario experiments

	Control	2 × CO ₂	3 × CO ₂
Northeastward	4.48	4.75	4.49
Zonal	3.12	3.08	3.09
Stationary	4.55	4.24	4.49
Total	12.15	12.07	12.07

the centroids and their occupation numbers differ. In order to assess a climatic change of the relative trajectories, the method is changed to obtain common centroids.

Therefore, the cluster analysis is applied to the combination of the tracks of all three experiments to obtain a single set of centroids. These centroids are similar to Fig. 8 and are not shown. The occupation numbers for the three scenario experiments and the three clusters reveal the distribution of the orientations changing in different climates. Table 2 gives the occupation numbers per month for the three cyclone regimes and the three experiments. Major differences between the clusters are found only in the 2 × CO₂ simulation: the number of northeastward cyclones is increased by 6% at the expense of the stationary cyclones. In the 3 × CO₂ run, however, the occupation numbers remain unchanged compared to the control run. The changes in 2 × CO₂ and 3 × CO₂ are not significant according to a χ^2 -test.

5 Summary and discussion

Time slice simulations based on coupled scenario experiments are analysed to assess the influence of an increased greenhouse gas concentration on the frequency, intensity, and direction of North-Atlantic cyclones. Three simulations with the 2.8° × 2.8° resolution model ECHAM3 for 1 ×, 2 × and 3 × CO₂ concentrations are compared. The classical storm track analysis (based on the geopotential height variance) and a Lagrangian cyclone tracking algorithm (locating the paths of geopotential height minima) are applied. The North-Atlantic storm track intensifies at the downstream end in the 2 × CO₂ run, and at the southeastern end in the 3 × CO₂ run. The following features of the cyclones in the scenario simulation are found:

1. The cyclone *frequency* of the control run agrees well with observations. In comparison with the control run, the cyclone frequency shifts northeastward in the 2 × CO₂ simulation, and northward in the 3 × CO₂ simulation. These signals cannot be identified in the storm track eddy statistics. However, the 2 × CO₂ and 3 × CO₂ cyclone frequency anomalies are both related to the mean geopotential height

response. The shift of the cyclone frequency is noted also in the study of Lunkeit et al. (1996), but not in the analysis of Carnell et al. (1996).

2. The cyclone *intensities* are not altered in the scenario runs. Here, the intensity is measured by the geopotential height gradient and not by the central pressure changing with the location of the cyclone. Our result differs from other studies, which find an intensity reduction (Beersma et al. 1997) or an increase (Lunkeit et al. 1996), but agrees with observations (von Storch et al. 1993).
3. Regimes of the *orientation* of relative cyclone trajectories are distinguished by a recently introduced cluster analysis. There are three North-Atlantic cyclone track clusters which are characterised by a stationary, zonal, and northeastward orientation. The centroids and their occupation numbers in the control run agree well with the observations. The change of cyclone properties in the scenario experiments is assessed by a combined cluster analysis of all tracks of the three runs. Only the number of northeastward propagating cyclones increases in the 2 × CO₂ experiment at the expense of stationary cyclones, whereas the total numbers remain unchanged. This is in agreement with the northeastward shift of the cyclone frequency.

So far, there seems to be no general agreement between the different model simulations on the effect of the influence of increased greenhouse gases on the Northern Atlantic cyclonic activity. The models differ mainly with respect to resolution, physical parametrisations, and the representation of the ocean, ranging from constant SST boundary conditions up to a comprehensive ocean circulation model. Although the models agree reasonably well in the predicted mean temperature anomalies (first moments), the anomalies of the variability show a wide spread. In general, the models disagree in the sense that the storm track response is weak or negligibly small, sometimes even changing sign in different simulations. Therefore, in order to assess climate change it might be useful to consider not only the storm track but also other quantities related to the cyclonic intensity. In this publication we consider cyclones and their paths to analyse directly the variability and possible anthropogenic changes of synoptic weather systems. There appears to be no direct relation between the storm track intensity and the cyclone frequency. On the one hand anticyclones are present in the storm track statistics and on the other an intensification of the zonal flow reduces the number of lows but not the variance.

The results for the cyclone frequency show similar contradictory properties in the different studies. Most of them are restricted to the counting of lows using some criteria for the identification of intense systems, with different ways to count occurrences at adjacent time steps. Fewer studies apply cyclone tracking to improve the assessment of the synoptic systems.

Cyclone tracking depends on even more details like the identification of the lows, the tracking method (compare e.g. Hodges 1994), the minimum lifetime, and the search range. The latter may vary with the geographical region, the spatial, and temporal resolution of the data. Not only the determination of a control climatology but also the calculation of anomalies may cause errors. A northward shift of cyclone trajectories, for example, may be systematically overlooked if the search range decreases northward, leading to interrupted tracks; which are then neglected due to the minimum lifetime condition. This clearly shows that results for the trajectories with different methods are barely comparable.

Our results for the storm track variance and the cyclone frequency reveal distinct anthropogenic modifications. The results show that in the near-polar region, the mean 1000 hPa geopotential height response is a reliable indicator for the modification of the cyclone frequency in the scenario experiment. In this region, however, the classical 500 hPa geopotential height variance appears to be not relevant. The findings for the changes of the cyclone frequency are substantiated by the cluster analysis of the relative cyclone trajectories. The centroids of the cluster analysis represent types of cyclones with characteristic physical properties and geographical preferences. Thus, the cluster analysis is a useful tool to describe the variability within the storm track and to interpret the response in terms of synoptic characteristics.

Acknowledgements We would like to thank the two referees for their helpful comments. This work was supported by the European Community under contract EV5V-CT94-0503 and the Bundesministerium für Bildung, Wissenschaft, Forschung und Technologie (07VKV01/1).

References

- Beersma JJ, Rider KM, Komen GJ, Kaas E, Kharin VV (1997) An analysis of extra-tropical storms in the North Atlantic region as simulated in a control and $2 \times \text{CO}_2$ time-slice experiment with a high-resolution atmospheric model. *Tellus* 49A: 347–361
- Blackmon ML (1976) A climatological spectral study of the 500 mb geopotential height of the Northern Hemisphere. *J Atmos Sci* 33: 1607–1623
- Blender R, Fraedrich K, Lunkeit F (1997) Identification of cyclone track regimes in the North Atlantic. *Q J R Meteorol Soc* 123: 727–741
- Carnell RE, Senior CA, Mitchell JFB (1996) An assessment of measures of storminess: simulated changes in Northern Hemisphere winter due to increasing CO₂. *Clim Dyn* 12: 467–476
- Cubasch U, Hasselmann K, Höck H, Maier-Reimer E, Mikolajewicz U, Santer BD, Sausen R (1992) Time-dependent greenhouse warming computations with a coupled ocean-atmosphere model. *Clim Dyn* 8: 55–69
- Cubasch U, Santer BD, Hellbach A, Hegerl GC, Höck H, Maier-Reimer E, Mikolajewicz U, Stössel A, Voss R (1994) Monte Carlo climate change forecast with a global coupled ocean-atmosphere model. *Clim Dyn* 10: 1–19
- Cubasch U, Waszkewitz J, Hegerl G, Perlwitz J (1995) Regional climate changes as simulated in time slice experiments. *Clim Change* 31: 273–304
- Flohn H, Kapala A, Knoche HR, Mächel H (1992) Water vapour as an amplifier of the greenhouse effect: new aspects. *Meteorol Z, NF* 1: 122–138
- Fraedrich K, Grothjahn R, Leslie LM (1990) Estimates of cyclone track predictability, II: fractal analysis of midlatitude cyclones. *Q J R Meteorol Soc* 116: 317–335
- Fraedrich K, Bantzer C, Burkhardt U (1993) Winter climate anomalies in Europe and their associated circulation at 500 hPa. *Clim Dyn* 8: 161–175
- Gates WL (1992) AMIP: the atmospheric model intercomparison project. *Bull Am Meteorol Soc* 73: 1962–1970
- Hall NMJ, Hoskins BJ, Valdes PJ, Senior CA (1994) Storm tracks in a high resolution GCM with doubled carbon dioxide. *Q J R Meteorol Soc* 120: 1209–1230
- Hayden BC (1981) Cyclone occurrence mapping: equal area or raw frequencies? *Mon Weather Rev* 109: 168–172
- Hegerl GC, von Storch H, Hasselmann K, Santer BD, Cubasch U, Jones PD (1996) Detecting greenhouse-gas-induced climate change with an optimal fingerprint method. *J Clim* 9: 2281–2306
- Hodges KI (1994) A general method for tracking analysis and its application to meteorological data. *Mon Weather Rev* 122: 2573–2586
- IPCC (1990) *Climate Change. The IPCC Scientific Assessment.* Cambridge University Press for the Intergovernmental Panel on Climate Change (1st edn), Cambridge, UK, 365pp
- IPCC (1992) *Climate Change 1992: The supplementary report to the IPCC Scientific Assessment.* Prepared by IPCC Working Group I, Houghton JT, Callander BA and Varney SK (eds), and WMO/UNEP. Cambridge University Press, Cambridge, UK, 200 pp
- König W, Sausen R, Sielmann F (1993) Objective identification of cyclones in GCM simulations. *J Clim* 6: 2217–2231
- Lambert SJ (1995) The effect of enhanced greenhouse warming on winter cyclone frequencies and strengths. *J Clim* 8: 1447–1452
- Lambert SJ (1996) Intense extratropical Northern Hemisphere winter cyclone events: 1899–1991. *J Geophys Res* 101: 21319–21325
- Lunkeit F, Ponater M, Sausen R, Sogalla M, Ulbrich U, Windelband M (1996) Cyclonic activity in a warmer climate. *Contrib Atmos Phys* 69: 393–407
- Maier-Reimer E, Hasselmann K (1987) Transport and storage of CO₂ in the ocean – an inorganic ocean-circulation carbon cycle model. *Clim Dyn* 2: 63–90
- Perlwitz J (1997) Zeitscheibenexperimente mit dem atmosphärischen Zirkulationsmodell T42-ECHAM3 für eine verdoppelte und verdreifachte CO₂-Konzentration unter besonderer Beachtung der Änderungen der nordhemisphärischen troposphärischen Dynamik. PhD-thesis, Universität Hamburg, Germany
- Roeckner E, Dümenil L, Kirk E, Lunkeit F, Ponater M, Rockel B, Sausen R, Schlese U (1989) The Hamburg version of the ECMWF model (ECHAM). In: Boer GJ (ed), *Research activities in atmospheric and oceanic modelling*, vol. 13. pp 7.1–7.4. CAS/JSC Working Group on Numerical Experimentation, WMO/TD 322, WMO, Geneva
- Roeckner E, Arpe K, Bengtsson L, Brinkop S, Dümenil L, Esch M, Kirk E, Lunkeit F, Ponater M, Rockel B, Sausen R, Schlese U, Schubert S, Windelband M (1992) Simulation of the present-day climate with the ECHAM model: impact of model physics and resolution. MPI-Rep 93, Max-Planck-Institut für Meteorologie, Hamburg, Germany
- Schinke H (1993) On the occurrence of deep cyclones over Europe and the North Atlantic in the period 1930–1991. *Contrib Atmos Phys* 66: 223–237
- Siegmund PC (1990) The effect of a doubling of atmospheric CO₂ on the storm tracks in the climate of a general simulation model. *KNMI Sci Rep*, WR 90–01, 33pp

- Stephenson DB, Held IM (1993) GCM response of northern winter stationary waves and storm tracks to increasing amounts of carbon dioxide. *J Clim* 6:1859–1870
- von Storch H, Guddall J, Iden KA, Jónsson T, Perlwitz J, Reistad M, de Ronde J, Schmidt H, Zorita E (1993) Changing statistics of storms in the North Atlantic. Rep 116, Max-Planck-Institut für Meteorologie, Hamburg, Germany, 19 pp
- Zhang Y, Wang W-Ch (1997) Model-simulated northern winter cyclone and anticyclone activity under a greenhouse warming scenario. *J Clim* 10:1616–1634
- Zishka KM, Smith PJ (1980) The climatology of cyclones and anticyclones over North America and surrounding ocean environs for January and July, 1950–77. *Mon Weather Rev* 108:387–401